Bioprocess Monitoring: A Moving Horizon Estimation Experimental Application ⋆

Andrea Tuveri * **Haakon Eng Holck** * **Caroline S.M. Nakama** * **José Matias** * **Johannes Jäschke** * **Lars Imsland** ** **Nadav Bar** *

* *Department of Chemical Engineering, Norwegian University of Science and Technology (NTNU), Trondheim, Norway (e-mail: nadi.bar@ntnu.no)*
** *Department of Engineering Cybernetics, Norwegian University of Science and Technology (NTNU), Trondheim, Norway*

Abstract: Microbial fermentation processes are most often described by nonlinear time-varying dynamics, which require the implementation of nonlinear state estimators to infer unmeasured metabolites in the cultivation broth. Among the various nonlinear available estimator strategies, the Moving Horizon Estimator (MHE) is an *on-line* optimization approach that easily allows to enforce hard constraints, an important feature that helps to avoid unfeasible concentrations. In this work we implemented an MHE by using experimental data from a fed-batch cultivation process of *Corynebacterium glutamicum*. Available real-time measurements of biomass and CO_2 formation were used to infer sugar concentrations by combining the available measurements with a simple Monod model. We found that the MHE was able to estimate all the three variables of interest, including the unmeasured sugar concentrations, during the entire fed-batch cultivation process. Moreover, we show that the estimates are accurate in comparison to the reference *off-line* samples. This work demonstrates the benefits of MHE as a soft sensor that can monitor bioprocesses in real-time.

Keywords: Estimation and control in biological systems, Parameter and state estimation, Monitoring, Optimization

1. INTRODUCTION

Automation of biological processes is limited due to the unavailability of *on-line* measurement devices that can quantify variables of interest. The lack of sensors can be circumvented by implementing state estimators that enable to monitor the process in real-time. These state estimators are dependent on mathematical models (Rao, 2000) that represent the system in a simplified manner (i.e. Monod growth model). Different applications of nonlinear estimation techniques, including Extended Kalman Filters (EKFs), Particle Filters (PFs) and Unscented Kalman Filters (UKFs), are available, as reported in Tuveri et al. (2021). However, those applications are all based on recursive Bayesian estimators, which approximate the posterior conditional probability density function (*pdf*) using measurements available at the current sampling instant.

Differently from them, optimization-based methods such as the Moving Horizon Estimator (MHE) use a moving window of past data (Robertson et al., 1996; Rawlings and Bakshi, 2006; Bavdekar et al., 2013; Ali et al., 2015). Most importantly, from a practical point of view and in contrast to the recursive Bayesian estimators, the MHE has:

- the ability to explicitly incorporate bound constraints in states and parameters;
- the possibility to easily handle multi-rate measurements;
- higher computational times (CPU times).

Indeed, MHE has the ability to explicitly incorporate physical constraints on states and parameters, and disturbances in the form of time-varying parameters can be added as extra degrees of freedom in the optimization (Robertson et al., 1996; Rao et al., 2003; Kühl et al., 2011). On the other hand, the EKFs or UKFs methods require strategies like clipping (Haseltine and Rawlings, 2005) or other optimization-based methods (Kolås et al., 2009; Tuveri et al., 2021) to avoid the estimation of negative concentrations. Additionally, time-varying parameters and disturbances have to be included as additional states, without the possibility to constrain them within predefined boundaries. Moreover, many real-time systems incorporate measurement devices with various sampling rates and times. For instance, whereas some absorbance probes sample every 10 seconds, sugar measurements by high performance liquid chromatography (HPLC) can be acquired every 30-60 minutes. The MHE, by considering a window of past measurements, is of interest in the case of such multi-rate measurements (Elsheikh et al., 2021), since it easily allows to place them in an adequate position within the time horizon. For those reasons, the MHE is a promising approach within bioprocesses.

⋆ The project was funded by the Bio Based Industries Joint Undertaking (JU) under the EU's Horizon 2020 research and innovation programme - N^o 790507. J. Matias acknowledges financial support from the Norwegian Research Council, SUBPRO, grant number: 237893. C. S. M. Nakama acknowledges financial support from the Norwegian Research Council through FRIPRO Project SensPATH.

The continuously increasing interest in real-time optimal control has brought advances in *nonlinear* Model Predictive Control (NMPC) algorithms and consequently in MHE methods (Findeisen et al., 2007). Indeed, even though fewer results are available in the literature about MHE, it can be seen as the dual of Model Predictive Control (MPC), since they both share moving horizon approach and dynamic optimization. The pioneering work of Kühl et al. (2011) in fact, transferred a fast real-time iteration approach developed for NMPC to MHE, contributing to its feasibility in real-time.

Although some *in-silico* applications within bioprocess monitoring are available (Raïssi et al., 2005; Valipour and Ricardez-Sandoval, 2021; Bae et al., 2021; Elsheikh et al., 2021), the implementation of MHE combined with experimental data is almost non-existent and, to the best of our knowledge, it was only presented by Goffaux and Wouwer (2008). In Goffaux and Wouwer (2008) the authors present a robust receding horizon approach in the case of uncertain parameters, by selecting the worst parameter realization in a min-max optimization approach. To reduce the high computational demand, model linearization and monotonicity assumptions are required. Differently from the implementation in Goffaux and Wouwer (2008), our approach does not require linearisation or monotonicity of the model, parameter realisation is considered nominal and model uncertainty is a free variable minimized in the cost function. In order to demonstrate the benefits of MHE in bioprocess monitoring, we present an implementation of MHE using real experimental data of a fed-batch bacterial cultivation of *Corynebacterium glutamicum*, previously presented in Tuveri et al. (2021). The estimation performance obtained here by the MHE is accurate with respect to the *off-line* samples. Moreover, we demonstrate the incorporation of hard state constraints directly in the optimization formulation. This is an important advantage when the practitioner needs to avoid nonphysical estimates (i.e. negative concentrations).

2. INPUT AND OUTPUTS

The *on-line* output measurements were collected every 60 seconds and used by the estimator to measure biomass, volume and CO_2 respectively and to infer the unmeasured glucose composition. Signals from the absorbance probe were obtained in concentration units (0.05 - 4 CU) and than converted to g/L (cell dry weight, CDW) using a calibration curve as follows.

CU $\geq$ 0.9:

$$CDW_{CU} = 22.187 \cdot CU - 5.0991$$

CU $<$ 0.9:

$$CDW_{CU} = 11.124 \cdot CU + 0.66116$$

On-line CO_2 signals were obtained as measure of the composition in the outflow (0%–25%). The volume was calculated by integrating *on-line* the signals from the pumps, taking into account also the amount of volume taken for the *off-line* samples (8 mL/sample). The feeding profile is reported in Fig. 1. From here on we will define the two different phases as batch (from zero to the start of the feeding) and fed-batch or second batch (from the feeding on). More information about measurements and experimental setup are reported in Tuveri et al. (2021).

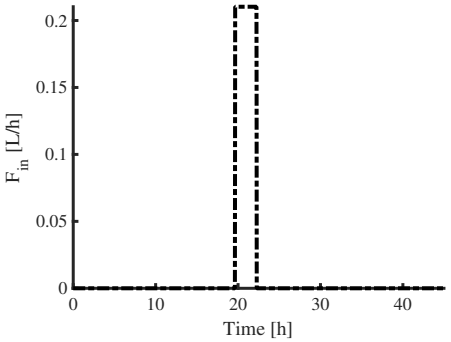

Fig. 1. Feeding profile.

3. SYSTEM MODEL

The dynamics are modelled by using simple Monod kinetics for growth on glucose as fed-batch process (Eq. 1), with the addition of linear cell death (Tuveri et al., 2021), where the state vector is defined by $x(t) = [V(t),\ X(t),\ S(t),\ CO_2(t)]^T$ and the input vector by $u = [F_{in}(t)]$. From here on we will drop the time-dependent notation for simplicity. The states V, X, S and CO_2 are respectively volume, biomass, substrate and carbon dioxide. F_{in} is the inflow of glucose with concentration S_{in} ($100g/L$), while q_{air} is the inflow of air (2 NL/min).

$$\begin{cases} \frac{dV}{dt} = F_{in} \\ \frac{dX}{dt} = -\frac{F_{in}}{V}X + \mu_{max}\frac{S}{K_s+S}X - k_dX \\ \frac{dS}{dt} = \frac{F_{in}}{V}(S_{in} - S) - \mu_{max}\frac{S}{K_s+S}\frac{X}{Y_{XS}} \\ \frac{d\mathrm{CO_2}}{dt} = \mu_{max}\frac{S}{K_s+S}\frac{X}{Y_{X\mathrm{CO_2}}} - q_{air}CO_2 \end{cases} \quad (1)$$

The parameters are μ_{max}, K_S, k_d, Y_{XS} and $Y_{X\mathrm{CO_2}}$ (Table 1). Those parameters were obtained using a nonlinear least-squares data fitting algorithm (lsqnonlin, Matlab) by a dedicated experiment (Tuveri et al., 2021).

Table 1. Values of model parameters (Eq. 1) with unit and standard deviations.

Parameter	Description	Value	Unit	Std. Dev.
μ_{max}	Maximum growth rate	0.19445	$[\mathrm{h}^{-1}]$	$3.25 \cdot 10^{-6}$
K_S	Monod growth constant	0.007	$[\mathrm{g \cdot L}^{-1}]$	$3.92 \cdot 10^{-6}$
k_d	Death rate constant	0.006	$[\mathrm{h}^{-1}]$	$4.49 \cdot 10^{-6}$
Y_{XS}	S from X yield	0.42042	$[\mathrm{g \cdot g}^{-1}]$	$3.58 \cdot 10^{-6}$
$Y_{X\mathrm{CO_2}}$	CO_2 from X yield	0.54308	$[\mathrm{g \cdot g}^{-1}]$	$2.22 \cdot 10^{-6}$

The covariance matrix for the parameters is calculated through the Fisher Information Matrix (FIM) as in Tuveri et al. (2021), where also structural identifiability and local observability for the system were positively assessed.

4. MOVING HORIZON ESTIMATION

The MHE estimates the states using past measurements at specific time points in the horizon $T = t_N - t_L$, where t_N represents the current time and t_L the starting point of the horizon. The time horizon is then discretized according to the sampling rate.

The dynamics of the process (Eq. 1) are described by a set of ordinary differential equations (ODEs):

$$\dot{x} = f(x, u, w) \quad (2)$$

$$y = h(x) \quad (3)$$

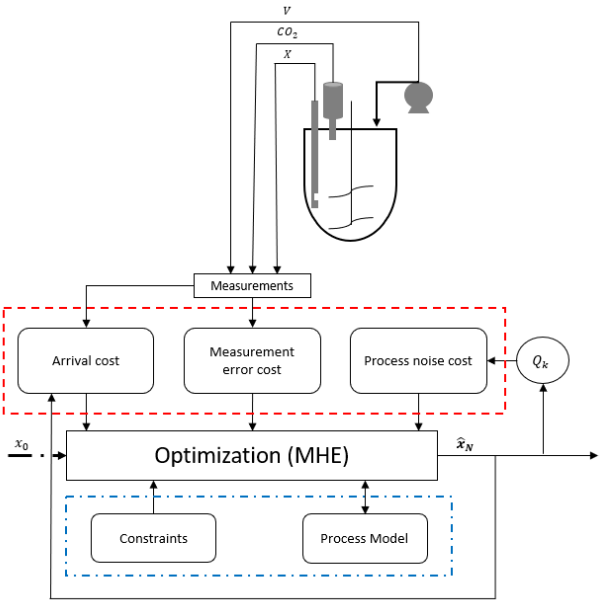

Fig. 2. The figure reports the MHE implementation, where the red dashed line represents the cost function (Eq. 6) and the blue dashed-dotted line its constraints. Measurements are given to both arrival and measurement error cost, while the measurement error covariance matrix is calculated at every iteration to weight for the model noise.

By discretizing it, we obtain:

$$x_{k+1} = F(x_k, u_k, w_k) \tag{4}$$
$$y_k = h(x_k) \tag{5}$$

where k denotes the sampling time t_k and w_k is a random variable.

The MHE problem (Kühl et al., 2011; Andersson et al., 2016) consists in finding the states and their noise obtained by solving the following constrained least-squares optimization problem:

$$\begin{aligned} \min_{x_i, w_i} \quad & \left(\|\hat{x}_L - x_L\|^2_{P_L} + \sum_{i=L}^{N} \|y_i - h(x_i)\|^2_V + \sum_{i=L}^{N-1} \|w_i\|^2_{W_k} \right) \\ \text{s.t.} \quad & x_{i+1} = F(x_i, u_i, w_i) \qquad i = L, \cdots, N-1 \\ & x_i \geq x_{min} \qquad i = L, \cdots, N \end{aligned} \tag{6}$$

The states x_i are constrained with $x_{min} = [0, 0, 0, 0]$ as a lower bound, to avoid negative (unfeasible) concentrations. Following the work of Kühl et al. (2011), we define:

$$P_L = P^{-1/2}, \qquad V = R^{-1/2}, \qquad W_k = {Q_k}^{-1/2} \tag{7}$$

and consider $\|b\|^2_B = b^T B^T B b$. The first term of the optimization (Eq. 6) is the arrival cost (Γ), which summarises the effect of measurements previous to the estimation horizon (up to t_L) and it is updated by single QR-factorization as in Kühl et al. (2011). The term $\hat{x}_L$ (Eq. 6) represents the optimal estimate of x_L.

The matrices P, R and Q_k (Eq. 7) are defined respectively as error, measurement noise and process noise covariances (Tuveri et al., 2021). Moreover, to take into account different process dynamics (Elsheikh et al., 2021), the process noise covariance Q_k is updated as in Tuveri et al. (2021). However since MHE, differently from EKF and UKF, takes into account several past measurements within the horizon T, the corresponding process noise covariance matrix Q_k is used for each sampling time (k) within the horizon. Along the optimization horizon (30 min), states (x_i) and process noise (w_i) are optimized using the information from the mechanistic model and the outputs (1 min sampling rate). The implementation of the MHE is illustrated in Fig. 2. To transform the continuous time model, we apply three point Legendre collocation on finite elements. The Nonlinear Programming (NLP) problem was solved using IPOPT (Wächter and Biegler, 2006) embedded in CasADi (Andersson et al., 2019).

4.1 Arrival Cost Update

Several approaches can be used to calculate the arrival cost. An interesting review on different arrival cost schemes and how they can effect the stability of the MHE is presented in Elsheikh et al. (2021). Here we describe the QR-factorization approach employed in this work, which approximates the arrival cost to a quadratic term that is updated before each new horizon (Kühl et al., 2011). Altough the QR-factorisation is a linearised technique as the EKF, it also holds all the numerical properties of the square-root Kalman Filter and the influence of past information can only grow within the limits of the process noise covariance Q_k (Kühl et al., 2011).

When we shift the horizon to a new start point at t_{L+1}, the arrival cost would ideally be defined as:

$$\begin{aligned} \Gamma(x_{L+1}) = \min_{x_L} \quad & \left(\|\hat{x}_L - x_L\|^2_{P_L} + \|y_L - h(x_L)\|^2_V + \|w_L\|^2_{W_L} \right) \\ \text{s.t.} \quad & x_{L+1} = F(x_L, u_L, w_L) \end{aligned} \tag{8}$$

However, since x_{L+1} is described by a nonlinear function, we do not have an analytical expression for the ideal arrival cost Γ. For obtaining an explicit solution of Eq. 8, some approximations are carried out. First, we define the term $x(t_{L+1}|x_L)$ as the solution of the ODEs (Eq. 4) in the interval from $t \in [t_L, t_{L+1}]$ with x_L as initial value. By linearizing $x(t_{L+1}|x_L)$ around the best available estimate x^*, we obtain:

$$\begin{aligned} x(t_{L+1}|x_L) &\approx x(t_{L+1}|x^*) + A \cdot (x_L - x^*) \\ &\approx \tilde{x} + A x_L \end{aligned} \tag{9}$$

where $\tilde{x} := x(t_{L+1}|x^*) - Ax^*$ and matrix A is the derivative of $x(t_{L+1}|x_L)$ with respect to x_L:

$$A = \left. \frac{\partial F(x_L, u_L)}{\partial x_L} \right|_{x^*}$$

Since in this case $h(x_L)$ is linear, we can represent it as $h(x_L) = Hx_L$, where H is a selector matrix. This way it becomes possible to solve, analytically, Eq. 8 by rewriting it as:

$$\min_{x_L} \left\| \begin{matrix} P_L(\hat{x}_L - x_L) \\ V(y_L - Hx_L) \\ W_L(x_{L+1} - \tilde{x} - Ax_L) \end{matrix} \right\|^2_2 \tag{10}$$

and transforming it using QR-factorization:

$$\begin{pmatrix} P_L & 0 \\ -VH & 0 \\ -W_L A & W_L \end{pmatrix} = \mathcal{Q} \begin{pmatrix} \mathcal{R}_1 & \mathcal{R}_{12} \\ 0 & \mathcal{R}_2 \\ 0 & 0 \end{pmatrix} \tag{11}$$

The QR-factorization decomposes the matrix in the objective function (Eq. 10) into the product of an orthogonal matrix $\mathcal{Q}$ and an upper triangular matrix $\mathcal{R}$ (Elsheikh et al., 2021). From Eq. 11, we then obtain an equivalent problem of the form:

$$\min_{x_L} \left\| \begin{pmatrix} \gamma_1 \\ \gamma_2 \\ \gamma_3 \end{pmatrix} + \begin{pmatrix} \mathcal{R}_1 & \mathcal{R}_{12} \\ 0 & \mathcal{R}_2 \\ 0 & 0 \end{pmatrix} \begin{pmatrix} x_L \\ x_{L+1} \end{pmatrix} \right\|_2^2 \tag{12}$$

The analytical solution of this problem (Eq. 12) results in the approximated quadratic expression for the arrival cost:

$$\Gamma^{'}(x_{L+1}) = \|\gamma_3\|_2^2 + \|\gamma_2 + \mathcal{R}_2 x_{L+1}\|_2^2 \tag{13}$$

Since the first term of Eq. 13 is given, the arrival cost updates are given by:

$$\hat{x}_{L+1} = -\mathcal{R}_2^{-1}\gamma_2, \qquad P_{L+1} = \mathcal{R}_2 \tag{14}$$

4.2 Moving Horizon Estimation Setup

The filter receives the signals from the sensors every 60 seconds. The states and the input of the system are defined in Section 3, while the measured outputs are:

$$y = [V \ CDW \ \mathrm{CO_2}]^T \tag{15}$$

The initial states are given by:

$$x_0 = [1.5 \ 1.2 \ 20 \ 0]^T$$

with initial covariance matrix:

$$P_0{}^+ = \begin{bmatrix} 2.09{\cdot}10^{-8} & 0 & 0 & 0 \\ 0 & 1.10{\cdot}10^{-5} & 0 & 0 \\ 0 & 0 & 1.09{\cdot}10^{-4} & 0 \\ 0 & 0 & 0 & 2.17{\cdot}10^{-5} \end{bmatrix}$$

and measurement noise covariance matrix R:

$$R = \begin{bmatrix} 10^{-2} & 0 & 0 \\ 0 & 10^{-1} & 0 \\ 0 & 0 & 10^{-3} \end{bmatrix}$$

The process noise covariance matrix Q_k was tuned as in Tuveri et al. (2021), where G_k is the Jacobian with respect to the model noise vector w:

$$G_k = \frac{\partial f(x, u, w)}{\partial w}$$

and Q_k is obtained as:

$$Q_k = G_k \cdot Q_w \cdot G_k{}^T \tag{16}$$

With Q_w defined as the covariance matrix of the noise w:

$$Q_w = diag\left[\ \sigma^2_{\mu_{max}} \ \sigma^2_{k_s} \ \sigma^2_{k_d} \ \sigma^2_{Y_{XS}} \ \sigma^2_{Y_{XCO_2}} \ \sigma^2_V \ \sigma^2_X \ \sigma^2_S \ \sigma^2_{CO_2}\ \right]$$

The values of Q_w are reported in Table 2. The values are kept equal to those reported in Tuveri et al. (2021), except the values for σ^2_V and $\sigma^2_{\mathrm{CO_2}}$, which have been modified as they are considered tuning parameters. The additive noise terms on the states are added to prevent the process noise covariance Q_k from being zero or indefinite whenever the substrate is depleted. To compensate for unmodelled dynamics, the values of $\sigma^2_{K_S}$ and $\sigma^2_{Y_{X\mathrm{CO_2}}}$ (Table 2) are increased, once the feeding phase is started and then kept constant thereafter.

Table 2. Variances (σ_i^2) of additive noise (w_i) in parameters and states. The parameters variance is obtained from Table 1. These values are kept constant until the second batch phase (Fed-batch values), when the values of $\sigma^2_{K_S}$ and $\sigma^2_{Y_{X\mathrm{CO_2}}}$ are increased to compensate for the unmodelled dynamics.

Variance	**Additive noise**	**Batch**	**Fed-batch**
$\sigma^2_{\mu_{max}}$	in μ_{max}	$1.05 \cdot 10^{-11}$	-
$\sigma^2_{K_S}$	in K_S	$1.54 \cdot 10^{-11}$	$3.38 \cdot 10^{-2}$
$\sigma^2_{k_d}$	in k_d	$2.02 \cdot 10^{-11}$	-
$\sigma^2_{Y_{XS}}$	in Y_{XS}	$1.28 \cdot 10^{-11}$	-
$\sigma^2_{Y_{X\mathrm{CO_2}}}$	in $Y_{\mathrm{XCO_2}}$	$4.91 \cdot 10^{-12}$	$4.91 \cdot 10^{-2}$
σ^2_V	in V	$1 \cdot 10^{-1}$	-
σ^2_X	in X	$1 \cdot 10^{-2}$	-
σ^2_S	in S	$1 \cdot 10^{-2}$	-
$\sigma^2_{\mathrm{CO_2}}$	in $\mathrm{CO_2}$	$1 \cdot 10^{-1}$	-

5. RESULTS

In this section, the estimation results (Fig. 3) for the system presented in Sec. 3 obtained by the application of the MHE with incorporation of state constraints (Sec. 4) are presented. The parameters were tuned as was presented in Sec. 4.2, while the time horizon was 30 minutes. As was reported in Tuveri et al. (2021), intracellular metabolic changes (e.g byproduct formation) during the batch and the feeding phases was not accounted for by the simple Monod model (because these changes are not entirely mapped), resulting in discrepancy between the model and the real dynamics. The results we obtained here (Fig. 3) are accurate with respect to the *off-line* measurements. The state estimator accurately follows the sugar consumption after adaptation of the tuning to the changes in metabolism due to high glucose feeding.

5.1 State Estimates

Using the MHE described in Sec. 4, we estimated with good accuracy the unmeasured glucose, following the changes in its concentrations also under high model mismatch (Fig. 3). It can be seen that the model predictions present a discrepancy compared to the *off-line* values. This is visible in both the first and the second (after feeding) batch. Despite these poor model predictions, the MHE improves the estimates by using the available information on the measurements.

Firstly, the *off-line* measurements of biomass are based on cell dry-weight, and are usually inaccurate due to manual sampling that exhibit high variance, e.g. at time $t = 8$ (Fig. 3a). The MHE, relying on the *on-line* OD high frequency measurements, estimated the biomass accurately compared to these *off-line* measurements, and at the same time corrected the biased biomass model prediction. Secondly, the consumption of the unmeasured sugars was well captured by the estimator, compared to the highly accurate sugar measurements (HPLC), even under high model-mismatch. Notably, the estimator could capture the change of sugar consumption rate after the feeding phase when we increased the parameters variance in the process noise covariance matrix Q_k. Thirdly, the model predictions for the CO_2 present the largest error. The CO_2 model predictions present a delay in the first

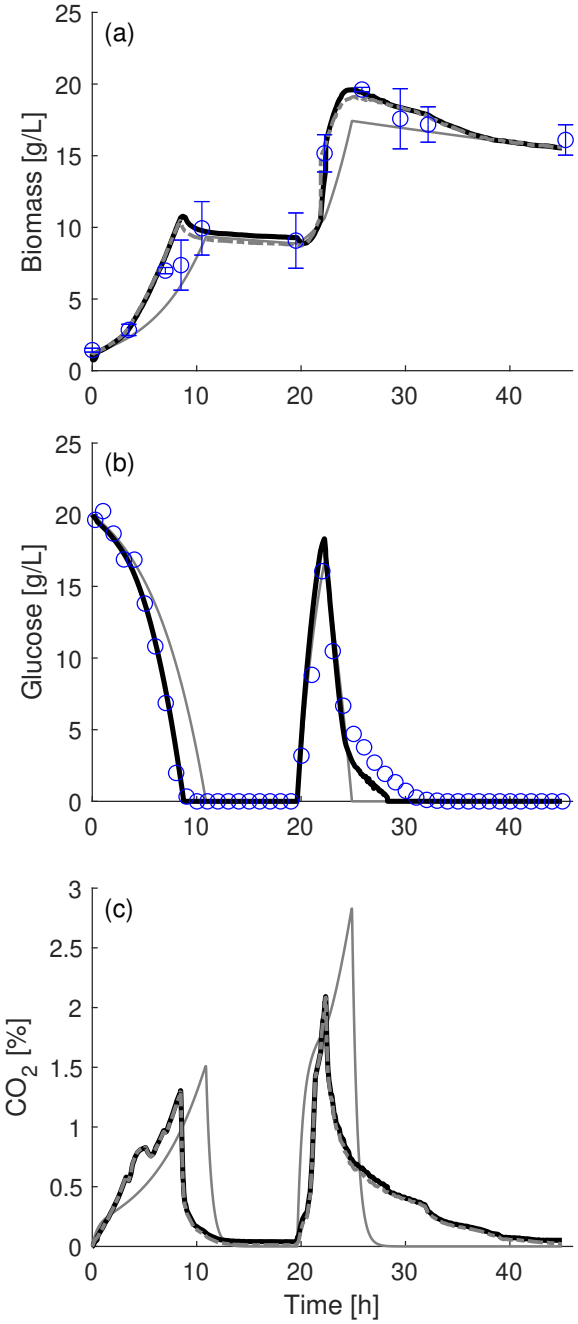

Fig. 3. Estimation results with 1 minute sampling interval. The blue circles (*off-line* measurements) and the dashed-dotted grey lines (sensor measurements) correspond to the experimental results. The solid grey is the open-loop model prediction and the solid black is the estimated value. The figures present the results for biomass (a), glucose concentrations (b) and CO_2 output (c). The MHE accurately estimated the states, and improved the estimate of the glucose compared to the model prediction.

batch and a high model mismatch in the second batch (feeding phase). However, this discrepancy is compensated by the MHE with the information on the measurements. Fourthly, it remains worth mentioning that similar results can be achieved by the application of recursive Bayesian state estimators (i.e. EKF and UKF) as shown in Tuveri et al. (2021). However, here we want to present the MHE

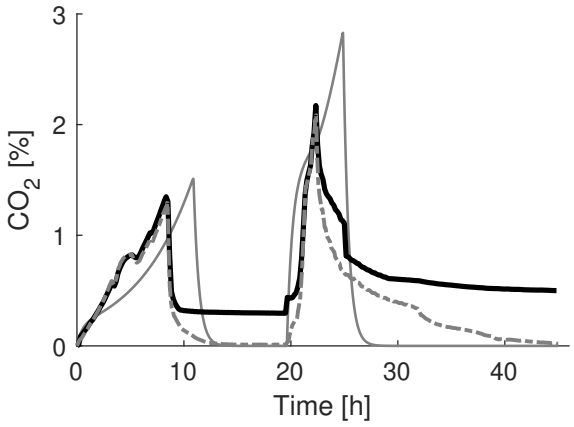

Fig. 4. Estimation results for the CO_2 output with a sampling interval of 10 minutes. The dashed-dotted grey lines (sensor measurements) correspond to the experimental results. The solid grey is the open-loop model prediction and the solid black is the estimated value. The estimated value presents a steady state offset.

as an alternative framework where constraints can be incorporated explicitly. Moreover, the reader must take into account that in this application the initial state vector x_0 was initialized by using the true states of the system at the initial time, given a certain initial error covariance matrix P_0 as in Tuveri et al. (2021). In the case of uncertain initial state vector x_0, the error covariance matrix would be initialized to a different value and the MHE would show slower convergence to correct the states. Our implementation of the MHE was dependent on the sampling frequency. The estimates of biomass X and CO_2 exhibited a steady state offset (Fig. 4) when the sampling rate was lower than 60 seconds. There are several explanations to that, and we will discuss two of them that we think are more relevant:

1) The tuning of the parameters R and Q_k weights differently the contribution of measurements and model information in the optimization problem. Indeed, tuning needs to be done after the frequency of the output measurements is defined. In our case we selected a sampling rate of 60 seconds as in Tuveri et al. (2021) and a relatively short horizon (30 minutes). We found that a short sampling interval combined with a sufficient horizon length improves the performance of the MHE, consistent with what reported in Schei (2008), where the author states that it is desirable to choose short sampling times intervals and a long data window. This is also consistent with what was reported in Haseltine and Rawlings (2005). Here the authors state that for short time horizons there is the possibility that the data within the horizon can not overcome the biasing of the arrival cost approximation. The tuning of the MHE presents therefore a compromise between performance and computational requirement (Schei, 2008), since longer time horizons imply a bigger optimization problem. However, the time it took to solve our optimization problem was in the interval 0.05 to 1 seconds, well within the time update interval (60 seconds).

2) Model mismatch can deteriorate the optimal solution, leading to steady-state offsets (Kühl et al., 2011). As it was presented previously (Elsheikh et al., 2021), due

to the complexity of biological systems, model mismatch is often encountered in bioprocesses and it can not be simply handled by a proper design of Q_k. Moreover, as already presented in Tuveri et al. (2021), the system under consideration presents a high model mismatch due to sudden metabolic changes after an exposure of the bacteria to high glucose concentration following an oxygen deprivation period. There are two possible remedies to this problem. One is to consider the system with unknown non-Gaussian uncertainties (through the use of a Gaussian mixture model) as was recently presented in Valipour and Ricardez-Sandoval (2022). Indeed the authors show how their approach is effective in cases involving either unexpected process or measurement (e.g. sensor drift) noises. The other is to include model parameters as decision variables in the optimization problem (Bae et al., 2021). Interestingly, the optimization problem will adapt the model (by adapting the parameter values) during the metabolic change periods. The inclusion of parameters as decision variables in the optimization problem may not only reduce the time for the practitioner to manually tune the MHE by trial and error, but also reveal possible changes in metabolic behaviors, leading to more robust models. However, if this is not coupled with a proper choice of parameter selection to optimize, it may lead to an ill-conditioned problem with over-fitted parameters, as previously discussed in Bae et al. (2021). This will be however part of further investigations.

6. CONCLUSION

This work presents the implementation of an MHE for the estimation of biomass, glucose concentrations and CO_2 formation in a fed-batch cultivation process. We reported here the efficacy of the MHE as an alternative state estimator in bioprocesses, demonstrating its advantage under necessity of hard state constraints. We showed that although the results were accurate with respect to the *off-line* measurements, simple tuning could not fully compensate for unmodelled dynamics. As a future work, the MHE has the potential to serve as a powerful tool that can both estimate the states in real-time and allow an adaptive parameter estimation. This will enable the detection of changes in metabolic behaviours and, as a consequence, the basis for more robust model predictions.

REFERENCES

Ali, J.M., Hoang, N.H., Hussain, M.A., and Dochain, D. (2015). Review and classification of recent observers applied in chemical process systems. *Computers & Chemical Engineering*, 76, 27–41.

Andersson, J.A.E., Gillis, J., Horn, G., Rawlings, J.B., and Diehl, M. (2019). CasADi: a software framework for nonlinear optimization and optimal control. *Mathematical Programming Computation*, 11(1), 1–36.

Andersson, L.E., Scibilia, F., and Imsland, L. (2016). An estimation-forecast set-up for iceberg drift prediction. *Cold Regions Science and Technology*, 131, 88–107.

Bae, J., Kim, Y., and Lee, J.M. (2021). Multirate moving horizon estimation combined with parameter subset selection. *Computers & Chemical Engineering*, 147, 107253.

Bavdekar, V.A., Gopaluni, R.B., and Shah, S.L. (2013). A comparison of moving horizon and Bayesian state estimators with an application to a pH process. *IFAC Proceedings Volumes*, 46(32), 160–165.

Elsheikh, M., Hille, R., Tatulea-Codrean, A., and Krämer, S. (2021). A Comparative Review of Multi-Rate Moving Horizon Estimation Schemes for Bioprocess Applications. *Computers & Chemical Engineering*, 107219.

Findeisen, R., Allgöwer, F., and Biegler, L.T. (2007). *Assessment and future directions of nonlinear model predictive control*, volume 358. Springer.

Goffaux, G. and Wouwer, A.V. (2008). Design of a robust nonlinear receding-horizon observer-Application to a biological system. *IFAC Proceedings Volumes*, 41(2), 15553–15558.

Haseltine, E.L. and Rawlings, J.B. (2005). Critical evaluation of extended Kalman filtering and moving-horizon estimation. *Industrial & engineering chemistry research*, 44(8), 2451–2460.

Kolås, S., Foss, B., and Schei, T. (2009). Constrained nonlinear state estimation based on the UKF approach. *Computers & Chemical Engineering*, 33(8), 1386–1401.

Kühl, P., Diehl, M., Kraus, T., Schlöder, J.P., and Bock, H.G. (2011). A real-time algorithm for moving horizon state and parameter estimation. *Computers & chemical engineering*, 35(1), 71–83.

Raïssi, T., Ramdani, N., and Candau, Y. (2005). Bounded error moving horizon state estimator for non-linear continuous-time systems: application to a bioprocess system. *Journal of Process control*, 15(5), 537–545.

Rao, C.V. (2000). *Moving horizon strategies for the constrained monitoring and control of nonlinear discrete-time systems*. The University of Wisconsin-Madison.

Rao, C.V., Rawlings, J.B., and Mayne, D.Q. (2003). Constrained state estimation for nonlinear discrete-time systems: Stability and moving horizon approximations. *IEEE transactions on automatic control*, 48(2), 246–258.

Rawlings, J.B. and Bakshi, B.R. (2006). Particle filtering and moving horizon estimation. *Computers & chemical engineering*, 30(10-12), 1529–1541.

Robertson, D.G., Lee, J.H., and Rawlings, J.B. (1996). A moving horizon-based approach for least-squares estimation. *AIChE Journal*, 42(8), 2209–2224.

Schei, T.S. (2008). On-line estimation for process control and optimization applications. *Journal of Process Control*, 18(9), 821–828.

Tuveri, A., Pérez-García, F., Lira-Parada, P.A., Imsland, L., and Bar, N. (2021). Sensor fusion based on Extended and Unscented Kalman Filter for bioprocess monitoring. *Journal of Process Control*, 106, 195–207.

Valipour, M. and Ricardez-Sandoval, L.A. (2021). Assessing the Impact of EKF as the Arrival Cost in the Moving Horizon Estimation under Nonlinear Model Predictive Control. *Industrial & Engineering Chemistry Research*, 60(7), 2994–3012.

Valipour, M. and Ricardez-Sandoval, L.A. (2022). A robust moving horizon estimation under unknown distributions of process or measurement noises. *Computers & Chemical Engineering*, 157, 107620.

Wächter, A. and Biegler, L.T. (2006). On the implementation of an interior-point filter line-search algorithm for large-scale nonlinear programming. *Mathematical programming*, 106(1), 25–57.